Nonlinear spectroscopy near half-gap in bulk and quantum well GaAs/AlGaAs waveguides

M. N. Islam and C. E. Soccolich
AT&T Bell Laboratories, Holmdel, New Jersey 07733

R. E. Slusher, A. F. J. Levi, and W. S. Hobson
AT&T Bell Laboratories, Murray Hill, New Jersey 07974

M. G. Young
AT&T Bell Laboratories, Holmdel, New Jersey 07733

(Received 30 August 1991; accepted for publication 1 November 1991)

We study the nonlinear properties of bulk AlGaAs and GaAs/AlGaAs multiple quantum wells (MQW) below the half-band-gap energy using subpicosecond pulses between 1.65 and 1.7 μm. In the bulk material we find a value for the nonlinear index $n_2 = +3.6 \times 10^{-14}$ cm^2/W and a two-photon absorption coefficient $\beta = 0.26 \times 10^{-4}$ cm/MW. In the MQW we measure an n_2 up to 2.4 times larger, and we attribute this enhancement to a stronger 1S-exciton intermediate state. The β value is up to 25 times larger in the MQW. This larger value may result from midgap states that resonantly enhance the virtual intermediate state in two-photon absorption and act as a real transition in a two-step absorption process. The resulting figure of merit ($2n_2/\beta\lambda$) for the bulk (MQW) material is 17 (1.6), which means that these semiconductors below half band gap are appropriate for all-optical switching and quantum optics applications. We confirm that n_2 is instantaneous on the 300 fs time scale of our pulses from self-phase-modulation spectra as well as time-resolved pump-probe measurements. However, we find an intriguing exchange of energy between the two orthogonal axes as evidenced by the signal along the probe axis following the negative derivative of the pump intensity. This result may be explained by self-phase modulation of the pump combined with a low-frequency Raman process that couples the modes along orthogonal axes.

I. INTRODUCTION

All-optical switching and quantum optics applications require materials that can provide a π-phase shift due to the nonlinear index with less than 3 dB of absorption. Although glass optical fibers have a relatively low nonlinearity, they are an almost ideal material for the nonlinear applications because of their extremely low loss. For example, ultrafast soliton logic gates[1] and squeezed states[2] have been demonstrated using optical fibers. However, these applications usually require long fiber lengths (e.g., >500 m), which implies latency as well as sensitivity to thermal and other environmental effects. The third-order nonlinear optical properties of semiconductors are of interest for making compact, integrable devices where many devices can be grown simultaneously on the same wafer. Several authors have shown that semiconductors are unsuitable for all-optical applications when excited between midgap and the band-gap energies because of nonlinear two-photon absorption (TPA).[3] In addition to generating real carriers that need to recombine, TPA leads to heating effects and in many cases limits the pump intensity so that a π-phase shift cannot be obtained.

In this article we investigate the nonlinear optical properties of bulk $Al_{0.2}Ga_{0.8}As$ and $GaAs/Al_{0.3}Ga_{0.7}As$ multiple quantum wells (MQW) at wavelengths below the half-band-gap energy. The GaAs/AlGaAs material system studied here is important for several reasons: (1) by varying the alloy composition the half-band-gap energy can cover the infrared window between 1.3 and 1.6 μm that is important for optical communications; (2) the material is almost perfectly lattice matched; and (3) already a very mature fabrication technology exists for these alloys. In addition, artificially structured, quasi-two-dimensional, MQW material has generated much interest because of unique linear and nonlinear properties. The reduced dimensionality of MQW's leads to more tightly confined 1S exciton wave functions, larger dipole matrix elements near the band edge, and unique electric field properties such as the quantum confined Stark effect.[4]

We present measurements of both the real and imaginary part of $\chi^{(3)}$ as well as time-resolved pump-probe data for both bulk and MQW material near 1.68 μm. In Sec. II we describe the experimental apparatus and details of the semiconductor samples. Self-phase-modulation spectra for the samples are discussed in Sec. III, and then the TPA measurements are given in Sec. IV. In Sec. V we provide evidence for midgap states in the MQW material, and in Sec. VI we describe pump-probe measurements. The results for the nonlinear index n_2 and TPA coefficient β show that these materials have favorable figures of merit for all-optical applications. The self-phase-modulation spectra as well as time-resolved pump-probe data prove that the response is instantaneous for 300 fs pulses. The pump-probe data also provide intriguing evidence for a low-frequency Raman process. We measure a maximum enchancement for n_2 of 2.4 times in MQW over bulk, which is consistent

 0021-8979/92/041927-09$04.00

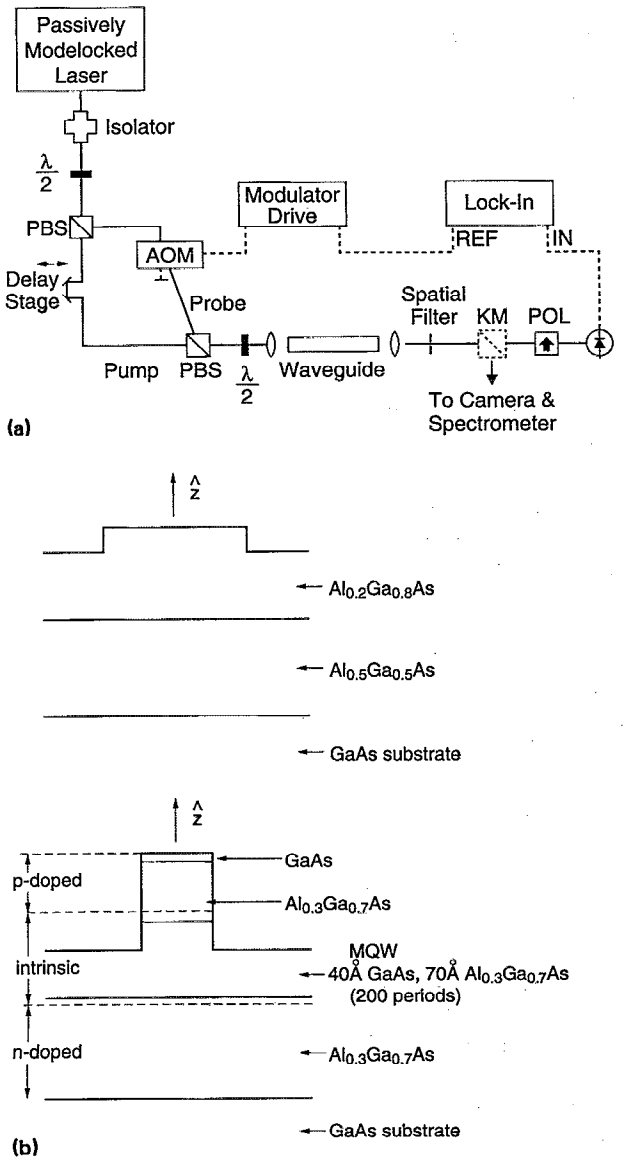

FIG. 1. (a) Experimental apparatus for testing semiconductor waveguides (PBS = polarizing beam splitter, AOM = acousto-optic modulator, KM = kinematic mount, POL = polarizer). Schematic of sample structures for (b) bulk and (c) MQW.

with enhancement of $\chi^{(3)}$ by the $1S$ intermediate excitonic state. The larger than expected increase in β in MQW over bulk may be partially attributed to midgap states.

II. EXPERIMENTAL APPARATUS AND SEMICONDUCTOR SAMPLES

A schematic drawing of the experimental apparatus is shown in Fig. 1(a). The laser source is a passively modelocked NaCl color center laser[5] that operates between 1.67 and 1.7 μm and produces 300 to 500 fs pulses separated by 11.4 ns. We use an optical isolator at the laser output to prevent feedback from the waveguide facets back into the laser. The laser output is separated into orthogonally polarized pump and probe beams, and the probe is frequency shifted by 80 MHz by passing through an acousto-optic modulator. A stepper-motor controlled delay line is used to vary the time separation between the two pulses, which are recombined at a polarizing beam splitter and then sent to the waveguides. A half wave plate placed before the waveguide allows selection of either the horizontal TE or vertical TM excitation. An antireflection coated laser diode objective lens is used to couple into the waveguide, and the output from the waveguide is collected with an identical objective and monitored on an IR camera. A spatial filter located near an intermediate focal plane at the output eliminates stray transmission adjacent to the guide. The frequency spectra of the output pulses are monitored with a grating spectrometer and the output pulse shapes are measured with an optical correlator.

We use waveguides (7 to 8.5 mm long) to obtain long interaction lengths and to enable access to both polarizations with respect to the quantum wells. In the MOCVD-grown bulk samples [Fig. 1(b)] a ridge waveguide is formed in a layer of $Al_{0.2}Ga_{0.8}As$ 2.55 μm thick. We choose this material composition so that the 1.6 μm wavelength excitation lies 100 meV below the half-gap energy ($\sim$1.5 μm), sufficiently far below to avoid TPA from all frequency components of the pulse.[6] Guiding is provided by a 2.55 μm underlying layer of lower index $Al_{0.5}Ga_{0.5}As$. The ridge height is 0.7 μm and its width is 4.5 μm for most of the measurements reported here. These dimensions were chosen so that simple optics could be used for coupling into the guide. The index difference is small enough so that only a few modes are supported by these waveguides and careful excitation results in the lowest-order mode dominating the transmitted light. Total coupling efficiencies of near 45% were obtained with microscope objectives at the input and output of the waveguide, and the total loss in the input and output microscope objectives is 6%. For the bulk sample both input and output surfaces are antireflection coated, thus reducing the reflections to near 1% per surface, and scattering from nonuniformities in the waveguide ridge is less than 5%. Peak powers as high as 300 W were measured at the output of the waveguide corresponding to peak intensities in the bulk waveguides near 10 GW/cm^2.

The MQW waveguides are grown in a different MOCVD reactor and the sample structure is included in Fig. 1(c). A *p-i-n* structure is formed by using a 0.2-μm-thick GaAs contact layer and a 1.5-μm-thick buffer layer of $Al_{0.3}Ga_{0.7}As$ that are *p* doped to a level of 10^{17} cm^{-3}. The intrinsic waveguide core consists of 200 periods of 40 Å GaAs wells and 70 Å $Al_{0.3}Ga_{0.7}As$ barriers. Guiding in the vertical dimension is assured by a 3-μm-thick layer of lower index $Al_{0.3}Ga_{0.7}As$ below the MQW guide region that is *n* doped to a level of 10^{17} cm^{-3}. Lateral confinement is provided by etching a 2-μm-wide ridge to a depth of 2.3 μm below the top surface of the wafer. We measure an overall linear transmission loss of approximately 9.14 dB, which includes 1.4 dB reflection loss per uncoated facet, 0.17 dB loss per objective, and an estimated 3 dB coupling loss. The excess loss of 3.2 dB in the MQW is attributed to scattering losses from nonuniformities along the waveguide ridge. For peak intensities near 11 GW/cm^2 in the waveguide peak powers of approximately

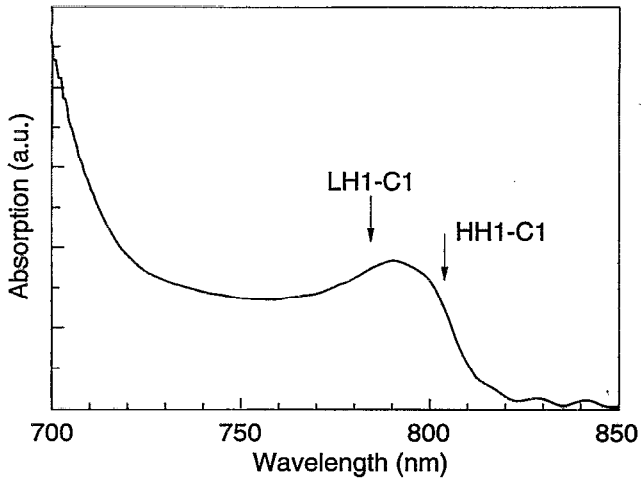

FIG. 2. Linear absorbance of MQW sample measured using white light transmission. The arrows mark the positions of the theoretically calculated transitions.

49 W for TE excitation and 32 W for TM excitation are measured at the output facet of the waveguide.

Figure 2 illustrates the MQW absorbance that is measured using white light transmission perpendicular to the layers ($\hat{e}_1\hat{z}$) after back-etching the GaAs substrate. We have calculated the confinement energies using a resonant tunneling procedure[4] assuming no overlap in wave functions between adjacent wells. We assume a 57:43 ratio for the hole:electron band offsets, and the formulas for the effective masses and band gaps are given in Ref. 4. For our MQW structure we calculate the lowest confinement energies of 31 meV for the heavy hole (HH1), 69 meV for the light hole (LH1), and 89 meV for the electron ($C1$). Therefore, the HH1-$C1$ transition should be at 1.544 eV (803 nm) and the LH1-$C1$ transition at 1.582 eV (784 nm). Careful examination of the transmission spectrum shows features near these wavelengths. The broadness of the exciton feature may be attributed to nonuniformity in well layer thickness or perhaps impurities within the quantum well layers. The absorption increases sharply at shorter wavelengths because of absorption in the AlGaAs buffer.

The TPA spectrum in MQW's has been shown to be highly anisotropic both experimentally[7] and theoretically.[8] The large anisotropies arise both from anisotropies of the exciton envelope function and an anisotropic band structure.[8] For the $\hat{e}\perp\hat{z}$ (electric field polarized in plane of wells, TE polarization) the TPA transition rate is nearly linear with $2\hbar\omega$-E_g and the strongly one-photon allowed $1S$ exciton is forbidden. Therefore, the $1S$ state of the HH1-$C1$ exciton at ~800 nm should be absent in the two-photon spectrum, and the effective band gap for TPA with $\hat{e}\perp\hat{z}$ should be about an exciton binding energy (~14–17 meV) above the $1S$ state, corresponding to ~1.56 eV (~795 nm). On the other hand, for $\hat{e}\parallel\hat{z}$ (electric field polarized perpendicular to wells, TM polarization) the TPA transition occurs at the LH2-$C1$ transition, which is even higher in energy, and the TPA spectra should display distinct steps. Our laser range from 1.66–1.7 μm should be at least 60 meV below the TPA edge for $\hat{e}\perp\hat{z}$ and even further away from the absorption edge for $\hat{e}\parallel\hat{z}$.

III. NONLINEAR INDEX FROM SELF-PHASE MODULATION

As in the case for optical fibers, we can use the simple self-phase-modulation spectral technique for measuring n_2 (Ref. 9) in our semiconductor waveguides. Self-phase modulation dramatically broadens the spectrum and forms a series of spectral peaks at phase shifts of π and larger for an instantaneous n_2 with negligible dispersion. The first null occurs at a 1.5π nonlinear phase shift, two nulls occur at 2.5π, etc. The nonlinear phase shift is given by

$$\Delta\Phi(t)=\frac{2\pi L_{\text{eff}}}{\lambda}n_2 I(t) \tag{1}$$

and the instantaneous change in the frequency is given by

$$\delta\omega(t)=-\frac{\partial\Delta\Phi}{\partial t}=-\frac{2\pi L_{\text{eff}}n_2}{\lambda}\frac{\partial I(t)}{\partial t}, \tag{2}$$

where L_{eff} is the effective length of the waveguide ($L_{\text{eff}}=[1-\exp(-\alpha L)]/\alpha$), λ is the vacuum wavelength, and $I(t)$ is the pulse intensity at the waveguide input. To obtain the spectral changes due to the nonlinear phase shift we perform the Fourier transform

$$\tilde{E}(\omega)=\frac{1}{2\pi}\int_{-\infty}^{\infty}E(t)\exp[i\Delta\Phi(t)]\times\exp[-i(\omega-\omega_0)t]dt, \tag{3}$$

where $E(t)$ is the electric field and $\tilde{E}(\omega)$ is the Fourier transform of the pulse amplitude (the measured spectra correspond to $|\tilde{E}(\omega)|^2$).

Figure 3 shows the experimental spectra at the output of the bulk waveguide as a function of power. The series in Fig. 3 corresponds to: (a) the input spectrum, (b) $\Delta\phi\cong\pi$, (c) $\Delta\phi\cong1.5\pi$, and (d) $\Delta\phi\cong2.5\pi$. Nearly identical spectra as a function of input intensity are obtained for wavelengths of 1.69 and 1.62 μm. Asymmetry of the spectra probably results from slight asymmetries of the input pulse shape. Similar spectra were measured for a probe beam orthogonally polarized with respect to the pump beam, and the probe intensity was maintained at one tenth of the pump intensity. In the bulk material the effective cross-phase modulation is two-thirds of the self-phase modulation as expected for the symmetry of the crystal. The intensity required for a π phase shift is 3.1 ± 0.5 GW/cm^2, which yields a value of $n_2=+3.6(\pm0.5)\times10^{-14}$ cm^2/W. The uncertainty in the measured values is primarily a result of estimating the pulse intensity in the multimode waveguide. The n_2 value is in qualitative agreement with the scaling predicted[10] near the TPA edge when compared with the measured value of $n_2=-4\times10^{-13}$ cm^2/W at a wavelength of 1.06 μm.[11] The sign of n_2 is positive for our waveguides, as deduced from the pulse broadening at high intensities. The sign of n_2 changes from negative to positive as one decreases the excitation energy from above to below the two-photon edge in agreement

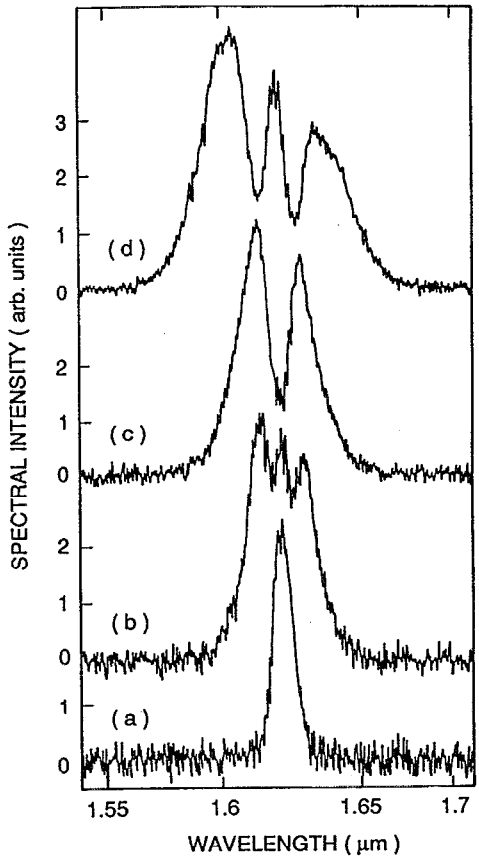

FIG. 3. Experimentally measured self-phase-modulation spectra at the output of the bulk waveguide as a function of increasing pump intensity. The series corresponds to: (a) the input spectrum, (b) $\Delta\Phi \simeq \pi$, (c) $\Delta\Phi \simeq 1.5\pi$, and (d) $\Delta\Phi \simeq 2.5\pi$.

with theoretical predictions.[10] Even at the large phase shift of 2π the measured nonlinear loss for the pump was only 15% in the bulk material.

Similar spectra are obtained in the MQW waveguides, except that we add a half-wave plate before the waveguide to rotate between $\hat{e}\perp\hat{z}$ and $\hat{e}\parallel\hat{z}$. Because of different absorption and since the MQW sample was not antireflection coated, the maximum nonlinear phase shift we obtained was about 1.5π. We are careful to use L_{eff} in Eq. (1) to deduce the value for n_2, and for the absorption coefficient α we use both the linear ($\sim$3 dB) and nonlinear losses, which are discussed in the next section. For $\hat{e}\perp\hat{z}$ we obtain a π-phase shift at $I = 5.2$ GW/cm^2, which corresponds to a value of $n_2 = +8.7(\pm 1.7) \times 10^{-14}$ cm^2/W. For $\hat{e}\parallel\hat{z}$ we find a π-phase shift at $I = 6.73$ GW/cm^2, which corresponds to a value of $n_2 = +5.4(\pm 1) \times 10^{-14}$ cm^2/W. Therefore, we find an enhancement for n_2 in the MQW of 2.4 (1.5) times the value in the bulk for $\hat{e}\perp\hat{z}(\hat{e}\parallel\hat{z})$. We attribute the larger nonlinearities to resonant enhancement from excitonic effects in the quasi-two-dimensional material. Since the enhancement will be localized to wavelengths close to the TPA edge, the measured n_2 for $\hat{e}\parallel\hat{z}$ is probably lower than the that measured for $\hat{e}\perp\hat{z}$ because our laser wavelength is further from the band edge when $\hat{e}\parallel\hat{z}$.

TPA can be described as a two-step process[12] that passes through an intermediate state and ends in an allowed state consistent with various selection rules. We concentrate on the $1S$ exciton as an intermediate state since this is strongly affected by the confinement, and the lowest-energy final state is the $2P$ exciton. Thus, the first photon induces a virtual interband transition to the $1S$ exciton with the second photon completing the electronic transition by an intraband transition to the $2P$ state.[7] There is no increase in binding energy or oscillator strength for the $n = 2$ state due to confinement,[7] so we do not expect a change in the intraband matrix element between the bulk and MQW at least for $\hat{e}\perp\hat{z}$.

If we consider only transitions through the $1S$-exciton intermediate state, then we expect the maximum enhancement factor to be proportional to the number of excitons that can be packed into the material. Therefore, the enhancement will be the volume of an exciton in three dimensions divided by the volume of an exciton in the quasi-two-dimensional material

$$\text{enhancement} \sim \frac{V_{\text{BULK}}}{V_{\text{MQW}}} \sim \frac{a_{3\text{D}}^3}{a_{2\text{D}}^2 L_w}, \tag{4}$$

where $a_{3\text{D}}$ ($a_{2\text{D}}$) is the three-dimensional (quasi-two-dimensional) Bohr radius and L_w is the well width. There may be additional prefactors in the right-hand side of Eq. (4); however, obtaining them requires a rigorous theoretical derivation, which is beyond the scope of this article.

The excitonic enhancement must be weighted by a filling factor to account for the fraction of the material in the wells. We will assume that the barriers have the same nonlinearity as in the bulk $n_2^{(\text{BULK})}$. Then, the material averaged nonlinearity is between

$$1 < \frac{n_2^{(\text{MQW})}}{n_2^{(\text{BULK})}} < \xi, \tag{5a}$$

where

$$\xi \simeq \frac{L_w}{L_t} \times \frac{a_{3\text{D}}^3}{a_{2\text{D}}^2 L_w} + \frac{L_b}{L_t} \times 1 \tag{5b}$$

and L_b is the barrier width and L_t is the period of the quantum wells ($L_t = L_w + L_b$). Note that although the well width cancels in Eq. (5b), it enters implicitly through the value of $a_{2\text{D}}$.

We now estimate ξ for our MQW samples with $L_w = 40$ Å, $L_b = 70$ Å, and $L_t = 110$ Å. In GaAs $a_{3\text{D}} = 140$ Å and Ref. 13 shows that $R_0 \times a_{3\text{D}}^2 \sim E_b \times a_{2\text{D}}^2$ is roughly a constant, where R_0 is the binding energy in three dimensions and E_b is the binding energy in the quasi-two-dimensional material. From Fig. 5 of Ref. 13 we find that for an aluminum content of $x = 0.3$ and $L_w = 40$ Å that $E_b \simeq 9.2$ meV, while $R_0 \simeq 4.2$ meV in GaAs. Therefore, we use $a_{2\text{D}} \sim a_{3\text{D}}\sqrt{R_0/E_b} \sim 95$ Å, which is the radius in the plane of the quantum well (the exciton looks like a "pancake"). Plugging these parameter values into Eq. (5) we calculate $\xi \simeq 3.4$, which should be peaked at wavelengths close to the TPA edge. We expect to observe less than the maximum enhancement since: (1) we are $\sim$60 meV away

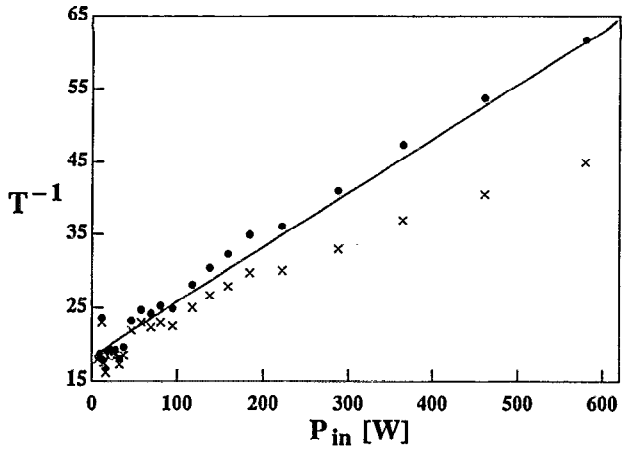

FIG. 4. Typical $1/T$ vs P_{in} curve measured at $\lambda = 1.67$ μm in the MQW sample for $\hat{e} \perp \hat{z}$. The $\times$'s correspond to the raw data, and the dots are obtained after correcting for the Gaussian temporal profile. The solid line is a least square error fit to the corrected data.

from the onset of TPA; and (2) the observed nonlinearity results not only from the $1S$-exciton intermediate state, but also through other states that are not as strongly confined. Therefore, our measured enhancement of 2.4 (1.5) for $\hat{e} \perp \hat{z}$ ($\hat{e} \| \hat{z}$) appears to be reasonable.

IV. TPA COEFFICIENT MEASUREMENT

To measure the TPA coefficient β in the MQW material, we measure the transmission of a single beam as a function of varied input intensity. Following the procedure in Ref. 3, we write

$$\frac{1}{T} = \frac{1}{T_0} + \frac{\beta L_{\text{eff}} P_{\text{inc}}}{C_{\text{out}} e^{-\alpha L} A_{\text{eff}}}, \tag{6}$$

where $T = I_{\text{trans}}/I_{\text{inc}}$ is the measured transmission, T_0 is the low intensity linear transmission, L_{eff} is the effective length of the waveguide, C_{out} is the coupling coefficient out

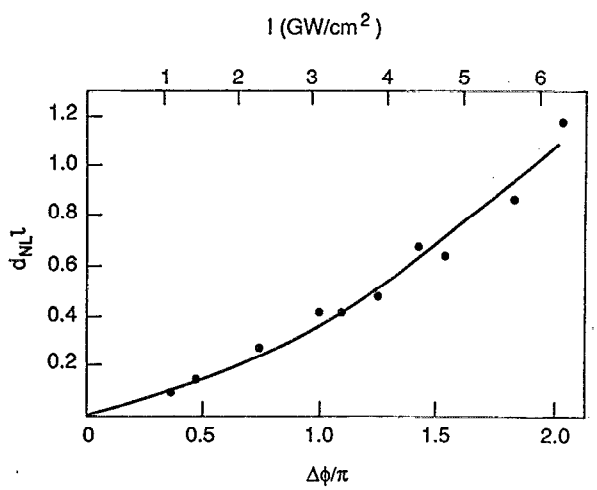

FIG. 5. Nonlinear absorption measured for a probe beam at an intensity one tenth of the pump intensity plotted as a function of nonlinear phase shift and pump intensity. The solid line is a fit to the data using Eq. (7).

of the waveguide, and A_{eff} is the effective area of the waveguide. We assume that $A_{\text{eff}} \simeq \frac{1}{2} A_{\text{geom}}$, which gives us an approximate spatial average over the mode profile. By plotting $1/T$ as a function of P_{inc} we can deduce β from the slope and T_0 from the intercept. In Fig. 4 we plot an exemplary $1/T$ vs P_{inc} curve taken at 1.67 μm. The raw data are plotted as $\times$'s and we obtain the dots after correcting for the Gaussian temporal pulse profile.[3] The corrected data would correspond to an experiment preformed with cw beams or square pulses.[14] A least square error fit to the corrected data is shown by the solid line, and the reasonable agreement of the linear fit with intensity confirms that TPA (or other $\chi^{(3)}$ processes) dominate the nonlinear loss mechanisms. We measured curves like Fig. 4 at four different wavelengths between 1.66 and 1.7 μm and deduced the corresponding β values. For the electric field polarized along the quantum wells $\hat{e} \perp \hat{z}$ we obtain an average value of $\beta = 6.5 \pm 1 \times 10^{-4}$ cm/MW, where the $\pm 15\%$ variation may be due to laser intensity fluctuations and varying pulse shapes from the laser at different wavelengths. There might also be a slight wavelength variation of β, but the scatter in our data does not show a definite trend. Along the orthogonal axis with $\hat{e} \| \hat{z}$ we obtain a lower average value of $\beta = 4 \pm 0.6 \times 10^{-4}$ cm/MW, which may be lower because we are further from the TPA band edge.

The nonlinear absorption is much weaker in our bulk material, so for a more accurate measure including three-photon absorption we study the nonlinear loss using a probe beam (Fig. 5). We measure the total (pump + probe) energy loss for the light propagating through the guide by measuring the 40 kHz modulation amplitude due to the probe as the pump is turned on and off. This measurement technique eliminates the need to correct for four-wave-mixing gain effects. We fit these data to

$$\alpha_{\text{NL}} = 4\beta \hat{I} + 9\alpha_3 \hat{I}^2, \tag{7}$$

where α_3 is the pump three-photon absorption coefficient and α_{NL} is the net nonlinear absorption coefficient for the signal beam. The fact that we measure a small signal absorption in order to obtain the pump absorption coefficients accounts for the factors of 4 and 9 in Eq. (7), and the intensities $\hat{I}$ in Eq. (7) are time averaged. Neither two-photon nor three-photon absorption alone yield a good fit to the data. The fitted values obtained are $\beta = 0.26 \times 10^{-4}$ cm/MW and $\alpha_3 = 0.004$ cm^3/GW^2. Unlike our MQW samples, the nonlinear absorption for phase shifts above 1.5π is dominated by three-photon absorption. Also, our measured three-photon absorption coefficient agrees with theoretical estimates[15] within a factor of 2. We did not measure the wavelength dependence of β for the bulk.

The 16 to 25 times larger values for β in the MQW samples is unexpected. The increase may indicate that we are closer to the TPA tail; i.e., in the bulk we are at least 100 meV below, while in the MQW we are $\sim$60 meV below for $\hat{e} \perp \hat{z}$ (even further for $\hat{e} \| \hat{z}$). However, we measure the TPA coefficient in the MQW to be almost flat as a function of frequency between 1.65 and 1.7 μm, whereas TPA through the Urbach tail of the band edge should decrease exponentially at longer wavelengths. Perhaps the

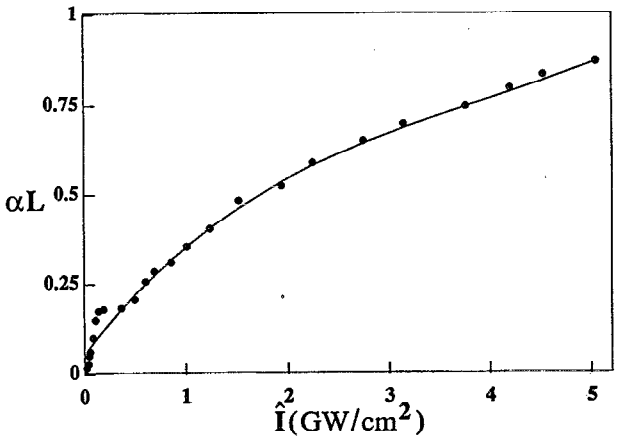

FIG. 6. Change in transmission of the probe with and without the pump ($\alpha L = -\ln[1 - \Delta T/T_0]$) for $\delta t < 0$ as a function of average pump intensity in the MQW waveguides. The dots correspond to the experimental data, and the solid line corresponds to a fit using Eq. (9).

enhanced β value in the MQW arises because of midgap or deep level states in the material, which act as a stepping stone in the TPA. The larger concentration of midgap states in the MQW may be due to interface states, higher levels of impurities, or differences in the MOCVD reactors in which the two samples were grown. Nonetheless, our measured values are more than a factor of 30 smaller than the $\beta = 0.02$ cm/MW measured well above the half-gap energies.[16]

V. EVIDENCE FOR MIDGAP STATES IN MQW

Further evidence that suggests the existence of midgap states in our MQW material is found from pump-probe measurements. The pump and probe beams are orthogonally polarized, and the time-resolved data will be presented in the next section. However, for the probe preceding the pump ($\delta t < 0$) we find a pronounced difference between the bulk and MQW material. Whereas in the bulk the transmission of the probe is unaffected by the presence of the pump, for the MQW there is a decrease in the probe transmission when the pump is added even for $\delta t < 0$. We found no thermal effects with time constants of the order of milliseconds. This long-lived background in the MQW is probably not due to free carriers because the carriers would diffuse out of the waveguide core in times shorter than the 11.4 ns separation between pulses. For example, for a Gaussian beam the diffusion decay time is given by

$$\tau_D = w_0^2/8D, \tag{8}$$

where D is the diffusion coefficient and w_0 is the Gaussian beam waist. We obtain $\tau_D = 0.38$ ns for $w_0 = 2$ μm and $D = 13$ cm^2/s, which is the ambipolar diffusion coefficient in the plane of the MQW layers for GaAs/AlGaAs MQW structures.[17]

To understand the origin of this long-lived background in the MQW material, we studied the change in transmission of the probe (with and without the pump) for $\delta t < 0$ as a function of pump power. In Fig. 6 we plot $\alpha L = -\ln[1 - \Delta T/T_0]$, which is the total pump-induced absorption coefficient, versus the average pump intensity at the waveguide input. The dots correspond to the experimental data, and the slope at low intensities is consistent with midgap states contributing to a two-photon process. The saturation may arise from the limited number of midgap states.

The data in Fig. 6 can be fitted well to a cubic function

$$\alpha L = \gamma_0 + \gamma_1 \hat{I} + \gamma_2 \hat{I}^2 + \gamma_3 \hat{I}^3, \tag{9}$$

where $\hat{I}$ is the average intensity in (GW/cm^2). The solid curve in Fig. 6 corresponds to Eq. (9) with the parameters: $\gamma_0 = 0.0563$, $\gamma_1 = 0.357$, $\gamma_2 = -0.0678$, and $\gamma_3 = 5.76 \times 10^{-3}$. If we compare Eqs. (7) and (9), then we can define an effective β for $\delta t < 0$ of $\beta(\delta t < 0) = \gamma_1/(4L) = 1.1 \times 10^{-4}$ cm^2/MW, which is smaller than the $\beta(\delta t \sim 0) = 6.5 \times 10^{-4}$ cm^2/MW that we discussed in Sec. IV. We can also define a saturation intensity for the TPA process [i.e., $\beta \simeq \beta_0/(1 + I/I_{\text{sat}})$], in which case we find that $I_{\text{sat}} \simeq -\beta/\alpha_3$. Again we obtain β and α_3 from comparison of Eqs. (7) and (9) with the result $I_{\text{sat}} \simeq 11.85$ GW/cm^2. The saturation of the TPA through the midgap states should be contrasted with the three-photon absorption for band-to-band transitions, which leads to an increase in the absorption with increasing intensity as in Fig. 5.

For our samples we speculate that the difference in MOCVD reactors used to grow the two samples may account for the higher level of MQW midgap states. For example, a slight amount of unpurged oxygen in the growth chamber can lead to many interface states, which are known to absorb near midgap. Furthermore, oxygen also has an absorption near 0.8 eV (1.55 μm). In addition, GaAs is known to have a distribution of deep level states between 0.6–0.9 eV centered about the half gap. For example, the EL2 defect is the dominant deep donor in undoped GaAs, and the fundamental state of EL2 has a level at 0.75 eV (1.65 μm).[18] We are further investigating the origin of the larger β value. In bulk material midgap states may have lifetimes of between 1–10 ns. On the other hand, in MQW if the electrons escape from the wells and become spatially separated from the ionized centers, then the lifetimes may extend into the microsecond range. This may be responsible for the long lifetime and high level of the background that we are observing in the pump-probe measurements.

It appears that the midgap states enhance the TPA in two ways. First, they act as a real transition in a two-step absorption process (one photon ionizes the state and a second creates a valence-band to midgap-state transition), which corresponds to the long-lived state. Second, the midgap states resonantly enhance the virtual intermediate state in the TPA, which corresponds to the instantaneous β contribution. The first term will not affect the instantaneous n_2, but we might expect the second term to have some contribution. Although we cannot rule out this additional enhancement, it may not be significant in our wavelength range because β due to midgap states is almost

flat as a function of frequency and the magnitude of n_2 varies as the logarithmic derivative of β.

VI. TIME-RESOLVED PUMP-PROBE MEASUREMENTS

To verify the instantaneous response of the nonlinearity and to examine the dynamics in the waveguide, we also perform time-resolved pump-probe measurements with 285 fs pulses at 1.67 μm. The probe beam is orthogonally polarized to the pump with an intensity of less than 1% of the pump. Any coherent interference effects between the two pulses should average to zero since the probe is frequency shifted by the acousto-optic modulator. Only the probe beam is modulated, and the signal from the detector at the waveguide output is fed to a lock-in that is referenced to the same modulation frequency. Three sets of data are collected as a function of pump power: (i) no polarizer to see the complete change in output due both to the pump and probe; (ii) polarizer at output along probe axis to see the change in probe due to the pump beam; and (iii) polarizer at output along pump axis to see the change in pump due to the probe.

Other than the previously discussed background for $\delta t < 0$ in the MQW, we observe the same kind of temporal behavior in the bulk and MQW. Therefore, to avoid complications from the long-lived background, we show here the pump probe data as a function of pump power for the bulk sample (Fig. 7). Note that although the three curves of each set in Fig. 7 are drawn on the same scale, the various data are displaced for ease of display. With no polarizer at the waveguide output we observe the expected behavior for two- and three-photon absorption. The signal follows the pump pulse and recovers to a level slightly below the original level. This tail persists for approximately 50–100 ps after the pump pulse. It probably arises from free-carrier absorption associated with the carriers excited by multiphoton absorption. Other than this tail the response is indeed instantaneous on the time scale of 285 fs, thus confirming the virtual nature of the TPA. In Fig. 8 we plot the normalized peak change in transmission ($\Delta T/T$) as a function of peak pump intensity at the bulk waveguide input. The behavior is similar to Fig. 5, thus reiterating that the net absorption dip is from two- and three-photon absorption. In the MQW waveguides we find this same curve is roughly linear in pump power, reflecting the fact that the TPA is much stronger than in the bulk and thereby masks the three-photon absorption.

When we add the polarizer to the waveguide output, the behavior becomes much more complicated in both the bulk and MQW. With the polarizer aligned with the probe axis, we obtain a signal that resembles the negative derivative of the pump pulse. In Fig. 8 we also include the peak-to-peak change $\Delta T/T$ versus pump intensity (T is the transmission of the probe pulse) and see a linear behavior, thus confirming that the derivative-like signal is due to a $\chi^{(3)}$ process. Note that when the probe rises above its level for $\delta t < 0$ that the probe experiences significant gain (as large as 15%) indicating a transfer of energy between the two axes.

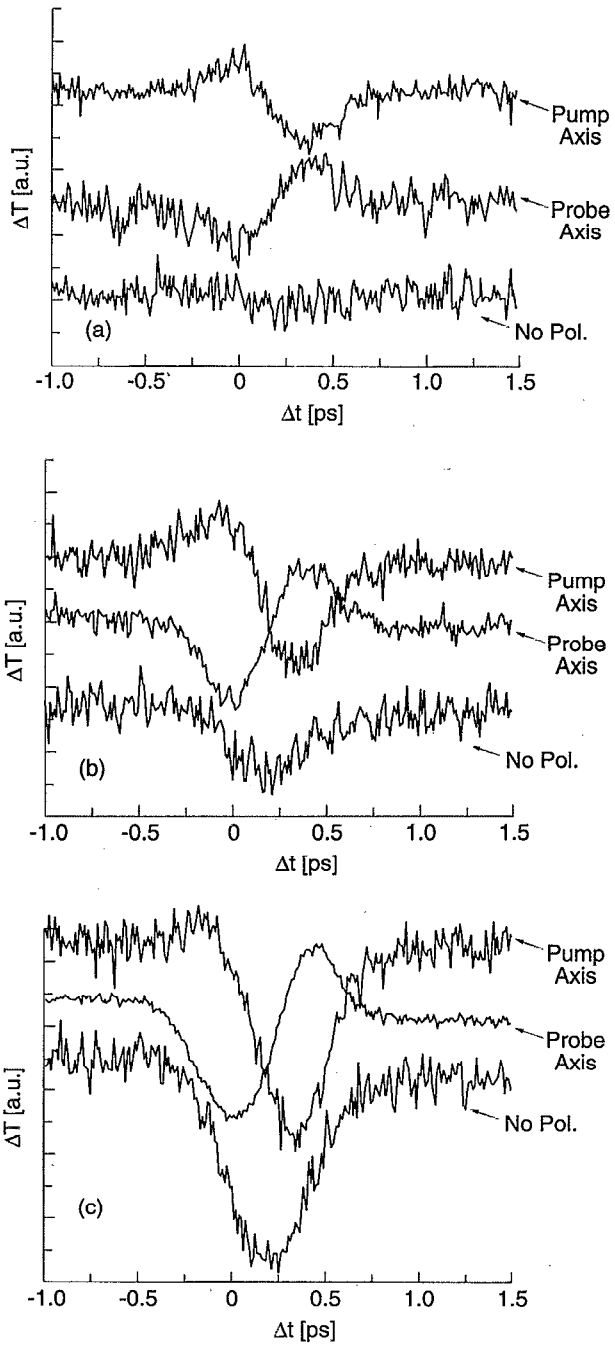

FIG. 7. Time-resolved pump-probe data using 285 fs pulses at 1.67 μm with no polarizer, polarizer at output along probe axis, and polarizer at output along pump axis. The pump intensity at the output of the bulk waveguide corresponds to: (a) 0.38; (b) 1.34; and (c) 3.85 GW/cm^2. Although the three curves in each set are drawn on the same scale, the various data are displaced for ease of display.

The third curve in each set corresponds to a polarizer at the waveguide output aligned with the pump axis. At low intensities where there is weak nonlinear absorption the change in pump looks like the negative of the change in the probe, and we see that the pump can be amplified by the probe. As the pump power is increased the dip in the signal increases as the nonlinear absorption increases. Since the changes along the two axes should add up to the signal without the polarizer, we see that the peak dip in

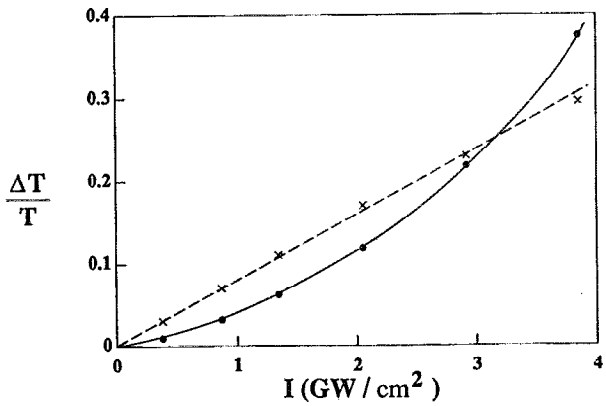

FIG. 8. Peak-to-peak change in transmission $\Delta T/T$ normalized to the probe transmission in the bulk waveguide as a function of output pump intensity. The solid dots correspond to no polarizer, and the ×'s correspond to a polarizer at the output along the probe axis.

transmission with the polarizer along the pump axis is delayed with respect to the dip with no polarizer.

How can four-wave mixing cause an exchange of energy between the two orthogonal axes? Self-phase modulation and cross-phase modulation only chirp pulses and do not change the number of photons along each axis. There are coherent four-wave mixing terms that give rise to polarization instability and phase conjugation,[19] but these terms are generally rapidly varying [proportional to $\exp(2i\Delta kz)$] and only become significant when $\Delta kL = 2\pi\Delta nL/\lambda \sim 1$, where Δn is the birefringence. We estimate the birefringence in our waveguides by including the material birefringence and calculating the effective index along both axes for our waveguide geometry. For the MQW waveguides we find $\Delta n \sim 2.5 \times 10^{-3}$ and for the bulk we obtain a lower value of $\Delta n \sim 7 \times 10^{-4}$. Even if we use the value for bulk material, the phase factor $\Delta kL \sim 20 \gg 1$, so the polarization instability terms should be unimportant. Also, despite the larger birefringence in the MQW sample, we observe comparable $\Delta T/T$ values in both the bulk and MQW samples. In addition, even if the coherent terms lead to a transfer of energy from the last 5% of the waveguide, we do not expect the signal to vary as the derivative of the pump pulse. Furthermore, since the coherent four-wave-mixing terms have different phase matching conditions along the two axes, we expect the behavior to depend on whether the pump is along the slow or fast axis. However, we have aligned the pump beam along the slow and fast axes of the MQW waveguides and observe the same qualitative behavior.

One possible explanation for the exchange of energy between the two axes is a low-frequency Raman gain. The Raman effect is equivalent to a time-dependent nonlinearity, and for the Raman effect the frequency separation should be on the order of a bandwidth of the pulse (~ 1 THz or 30 cm^{-1}). Consider a simple picture in which we assume that the pump spectrally broadens due to self-phase modulation and the Raman gain spectrum is linear down to low frequency. This situation is equivalent to a fiber with soliton self-frequency effect and cross-Raman effects except that the semiconductor waveguide has no walk-off over the short lengths.[20] Because of the Raman effect, when two pulses overlap, the lower frequency pulse experiences gain and depletes the other pulse. Recall from Eqs. (1) and (2) that the frequency chirp on the pump pulse behaves as $\delta\omega \propto -\partial I/\partial t$ for $n_2 > 0$; i.e., the leading edge ($\delta t < 0$) of the pump is red-shifted and trailing edge ($\delta t > 0$) is blue shifted. To lowest order we ignore the effects of cross-phase modulation and assume that the probe is at the original center frequency (the argument does not change if we include cross-phase modulation since the cross-phase-modulation coefficient is smaller than self-phase modulation). Then, for $\delta t < 0$, the probe is attenuated because it is higher in frequency that the pump, and for $\delta t > 0$ the probe is amplified because it is at a lower frequency than the pump. This is exactly the behavior observed in Fig. 7. More generally, this technique allows us to map out the chirp of the pump pulse along the probe axis.

We can estimate the Raman gain coefficient $R_\perp$ for orthogonally polarized pulses in the bulk material from the data in Fig. 8. For example, at $I \sim 3.85$ GW/cm^2 we obtain $(\Delta T/T)_{\max} \sim 0.3$, or the maximum gain is half of this $(\Delta T/T)_{\text{gain}} \sim 0.15$. In the small signal approximation we find that $R_\perp IL \sim (\Delta T/T)_{\text{gain}}$ or $R_\perp \sim 5.5 \times 10^{-11}$ cm/W. Since this intensity corresponds roughly to $\Delta\Phi \sim \pi$ and at a π-phase shift the frequency broadening is $\pm\Delta\nu$, where $\Delta\nu$ is the full width at half maximum pulse spectral width, this value of $R_\perp$ will be for $\Delta\nu \sim 1\text{THz} \sim 30\ \text{cm}^{-1}$. As we see in Fig. 7, the Raman effect is not negligible and is, in fact, comparable to two- and three-photon absorption in the bulk material.

VII. DISCUSSION

Based on our nonlinear measurements, we can now assess the appropriateness of these semiconductor materials below half gap for all-optical applications. In all-optical switching or quantum optics we require that $(\beta\lambda/2n_2) < 1$, i.e., that we obtain a π-phase shift with less than 3 dB of TPA. Alternately, we can define a figure of merit $F_m = 2n_2/\beta\lambda$ that must be greater than one. For the bulk $Al_{0.2}Ga_{0.8}As$ material we find that $F_m \simeq 17$, whereas for our MQW material we find that for both $\hat{e} \perp \hat{z}$ and $\hat{e} \| \hat{z}$ that $F_m \simeq 1.6$. For the MQW materials, at least, further improvements in the figure of merit must be obtained by decreasing the TPA coefficient. As we discussed before, the midgap absorption should not be fundamental to MQW material provided that caution is exercised during the growth to avoid impurities and interface states. Because of these favorable figures of merit, we have already used the bulk material in an all-optical time domain chirp switch,[21] which can be used for ultrafast logic or timing restoration in a soliton-based system. These waveguides should also be appropriate for proposed Mach-Zehnder devices[22] and squeezed state generation.[11]

Our comparison of bulk and MQW material also provides some guidelines as to the benefits expected from quantum confinement. Because of the enhancement through the 1S-exciton intermediate state, we expect the maximum enhancement in n_2 to be about 3.4 for our 40 Å

well and 70 Å barrier widths. In principle, the TPA coefficient for MQW should not be any worse than for bulk, so the maximum increase in F_m should also be of order 3.4. However, to observe this enhancement we must operate near the TPA edge, since only then the $1S$ exciton is involved in the process. One property of the MQW that might be useful is the anisotropy in the n_2 between the two axes.[7,8] Furthermore, it has been predicted[8] and demonstrated[23] that the TPA increases near the band edge for $\hat{e}\|\hat{z}$ with the addition of electric fields. Since the n_2 is related to the TPA spectrum through a Kramers–Kronig relation, the larger and sharper band edge implies a larger n_2 as well.

The pump-probe measurements shed new insight into the dynamics between the orthogonally polarized pulses. Although the response is primarily instantaneous, the derivative-like signal indicates the energy transfer between the two axes in addition to multiphoton absorption. We show that the exchange of energy between the two axes may be explained by self-phase modulation of the pump plus a low-frequency Raman gain, and the data implies a Raman coefficient between orthogonally polarized pulses of $R_\perp \sim 5.5 \times 10^{-11}$ cm/W for $\Delta\nu \sim 30$ cm^{-1}. GaAs is know to have sharp Raman modes near 300 cm^{-1} with very little contribution at low frequencies. There is low-frequency absorption associated with acoustic phonons, but Brillouin scattering generally requires phase matching while our observed phenomena (which occurs in different samples along different polarizations and at different pump powers) suggest a noncritical or self-phase-matched process. The situation is not as clear in alloy material such as AlGaAs, in which the alloy introduces new Raman lines and tends to broaden the spectrum. More importantly, since the alloy has random occupation of sites, the wave vector conservation rules for first-order Raman scattering in a perfect crystal will be relaxed[24] and there should be appreciable low-frequency Raman gain. In addition, even in the perfect crystal there are second-order Brillouin processes that involve two phonons and that behave Raman-like; i.e., wave vector conservation is satisfied by the difference between two acoustic phonon wave vectors. To our knowledge there is no report in the literature of the magnitude of the Raman gain coefficient in GaAs or AlGaAs, so we are unable to compare our results. On the other hand, our measured $R_\perp$ is at least two orders of magnitude larger than in fused silica fibers at comparable $\Delta\nu$, which is comparable to the enhancement of n_2 in the the semiconductor near half-gap.

In summary, we have measured the real and imaginary components of $\chi^{(3)}$ near the half-gap in bulk AlGaAs and GaAs/AlGaAs MQW waveguides. For the bulk material we find $n_2 = +3.6 \times 10^{-14}$ cm^2/W and $\beta = 0.26 \times 10^{-4}$ cm/MW, which imply a figure of merit $F_m = 17$. In the MQW we find that the nonlinearity for $\hat{e}\perp\hat{z}$ ($n_2 = +8.7 \times 10^{-14}$ cm^2/W) is enhanced by 2.4 times over the value in bulk, which is consistent with the maximum enhancement expected from the $1S$ intermediate state. We attribute the larger TPA coefficient ($\beta = 6.5 \times 10^{-4}$ cm/MW) in the MQW to midgap states, which cause a long-lived background in the pump-probe data for the MQW. Finally, time-resolved pump-probe measurements confirm that the nonlinearity is instantaneous and show that at least two mechanisms are responsible for the derivative-like behavior along the probe axis. We show that self-phase modulation plus a low-frequency Raman effect can explain the data, and we estimate the Raman gain coefficient $R_\perp$ around $\Delta\nu \sim 30$ cm^{-1}. Furthermore, this technique may be used to map out the chirp of the pump pulse along the probe axis.

We acknowledge stimulating discussions with S. Schmitt-Rink, D. A. B. Miller, J. P. Gordon, V. Mizrahi, J. Shah, R. H. Stolen, and T. Harris. Special thanks to K. W. Goossen for help in absorption measurements, and S. T. Ho was involved in the bulk nonlinear measurements.

[1] M. N. Islam, Opt. Lett. **15**, 417 (1990); M. N. Islam, Opt. Lett. **14**, 1257 (1989).
[2] K. Bergman and H. A. Haus, Opt. Lett. **16**, 663 (1991); M. Rosenbluh and R. M. Shelby, Phys. Rev. Lett. **66**, 153 (1991).
[3] V. Mizrahi, K. W. DeLong, G. I. Stegeman, M. A. Saifi, and M. J. Andrejco, Opt. Lett. **14**, 1140 (1989).
[4] D. A. B. Miller, D. S. Chemla, T. C. Damen, A. C. Gossard, W. Wiegmann, T. H. Wood, and C. A. Burrus, Phys. Rev. B **32**, 1043 (1985).
[5] M. N. Islam, E. R. Sunderman, C. E. Soccolich, I. Bar-Joseph, N. Sauer, T. Y. Chang, and B. I. Miller, IEEE J. Quantum Electron. **25**, 2454 (1989).
[6] S. T. Ho, C. E. Soccolich, M. N. Islam, W. S. Hobson, A. F. J. Levi, and R. E. Slusher, Appl. Phys. Lett. **59**, 2588 (1991).
[7] K. Tai, A. Mysyrowicz, R. J. Fischer, R. E. Slusher, and A. Y. Cho, Phys. Rev. Lett. **62**, 1784 (1989).
[8] A. Shimizu, Phys. Rev. B **40**, 1403 (1989).; A. Shimizu, T. Ogawa, and H. Sakaki, "Two-photon absorption spectra of low-dimensional semiconductors," presented at the Ninth International Conference on Electronic Properties of Two-Dimensional Systems, July 8–12, 1991, Nara, Japan.
[9] R. H. Stolen and C. Lin, Phys. Rev. A **17**, 1448 (1978).
[10] M. Sheik-Bahae, D. J. Hagan, and E. W. Van Stryland, Phys. Rev. Lett. **65**, 96 (1990).
[11] R. E. Slusher, S. L. McCall, A. Mysyrowicz, S. Schmitt-Rink, and K. Tai, in *Proceedings of the Symposium on Nonlinear Optics of Organics and Semiconductors* (Springer, Berlin, 1988), p. 24.
[12] G. D. Mahan, Phys. Rev. **170**, 825 (1968).
[13] S. Schmitt-Rink, D. S. Chemla, and D. A. B. Miller, Adv. Phys. **38**, 89 (1989).
[14] W. L. Smith, *CRC Handbook of Laser Science and Technology*, edited by M. J. Wever (CRC, Cleveland, OH, 1986), Vol. 3, Pt. 1.
[15] B. S. Wherrett, J. Opt. Soc. Am. B **1**, 67 (1984).
[16] M. J. LaGasse, K. K. Anderson, C. A. Wang, H. A. Haus, and J. G. Fujimoto, Appl. Phys. Lett. **56**, 417 (1990).
[17] P. W. Smith, Y. Silberberg, and D. A. B. Miller, J. Opt. Soc. Am. B **2**, 1228 (1985).
[18] J. Dabrowski and M. Scheffler, Phys. Rev. B **40**, 10 391 (1989).
[19] C. R. Menyuk, J. Opt. Soc. Am. B **5**, 392 (1988).
[20] C. R. Menyuk, M. N. Islam, and J. P. Gordon, Opt. Lett. **16**, 566 (1991).
[21] M. N. Islam, C. E. Soccolich, S. T. Ho, R. E. Slusher, W. S. Hobson, and A. F. J. Levi, Opt. Lett. **16**, 1116 (1991).
[22] A. Lattes, H. A. Haus, F. J. Leonberger, and E. P. Ippen, IEEE J. Quantum Electron. **QE-19**, 1718 (1983).
[23] K. Fujii, A. Shimizu, J. Bergquist, and T. Sawada, Phys. Rev. Lett. **65**, 1808 (1990).
[24] R. Shuker and R. W. Gamon, "Raman Scattering in Amorphous Materials," in *Scattering in Solids*, edited by M. Balkanski (Flammarion Sciences, Paris, France, 1971), p. 334.